Journal of Materials Chemistry B

COMMUNICATION

View Article Online
View Journal | View Issue

Cite this: J. Mater. Chem. B, 2019, 7, 1679

Received 28th July 2018,
Accepted 29th August 2018

DOI: 10.1039/c8tb01959b

rsc.li/materials-b

A shape-shifting composite hydrogel sheet with spatially patterned plasmonic nanoparticles†

Hongyu Guo,[a] Yijing Liu,[b] Yang Yang,[a] Guangyu Wu,[ac] Kerry Demella,[d] Srinivasa R. Raghavan[d] and Zhihong Nie*[a]

We report a simple and reliable approach to fabricate composite hydrogel sheets with spatially patterned regions of plasmonic gold nanoparticles using a combination of contact printing and diffusion-controlled galvanic replacement reaction. In response to near-infrared laser irradiation, the localized increase in temperature induced the controlled shape deformation of the composite hydrogels, due to the combined effect of photothermal heating of the loaded gold nanoparticles and the thermal responsiveness of the hydrogel matrix. The same hydrogel can be designed to exhibit different modes of shape deformation depending on the direction of light irradiation, which has rarely been reported previously. The composite hydrogels may find applications in biomedicine and soft robots.

Shape-changing materials have attracted considerable attention in the past few decades, owing to their potential applications in soft robots, artificial muscles, biomedicine and mechanical devices.[1–9] Among these materials, hydrogels, water-swollen networks, are unique since their deformation usually relies on a differential swelling in the material, which mimics naturally occurring shape-changing objects, such as tendrils, pine cones, Venus flytraps, *etc.*[1,2,7] Common strategies to generate differential swelling in hydrogels include layering materials that have varying swelling capability or generating domains within the hydrogel that have a swelling extent different from their surrounding materials.[1,7,8] Many environmental stimuli have been used to induce differential swelling in a hydrogel to trigger its deformation, such as temperature,[10–12] pH,[13] ionic strength,[14] enzymes,[15] DNA,[16] ions,[17] humidity,[18,19] light[20–22] and external fields.[23,24] Among others, light is particularly attractive as it can be remotely delivered to the material with desirable spatial and temporal resolution, which brings more controllability to the shape transformation of materials, such as liquid crystal polymer/elastomers,[25–34] shape memory films,[35–37] supramolecular assemblies,[38,39] and hydrogels.[20,21,40–45] For example, light can be used to drive the transformation of the same hydrogel sheet into multiple distinct shapes by modulating the light irradiation patterns,[40,41] which cannot be readily achieved by using chemical-responsive hydrogels.[46,47] Controllable motion of a shape-changing hydrogel can be realized by region-selective exposure of materials to light to induce shape deformation.[43,44] Despite the shape-transformation versatility enabled by local irradiation of light in these platforms, this strategy often requires a special set-up or is limited by undesired shape transformation originated from variation in the irradiation area upon the deformation of the materials.[41]

Instead of modulating the area of light exposure, one can structure the materials with light-responsive components and use un-patterned light to control the shape transformation of the material. This concept has been extensively used in the deformation of azobenzene-based materials in which the azobenzene moiety is pre-patterned in the materials, thus enabling defined deformation under light.[31,48] Another example is the shape transformation of pre-strained polystyrene films where the regions patterned with colored inks serve as actuation hinges in response to light.[37] In this case, the spatial distribution of the light responsive components is crucial to the mode and complexity of the shape transformation of the materials.[37] However, it remains challenging to readily control the distribution of light-responsive elements in materials simultaneously along both the in-plane and axial direction, in order to achieve more complex shape transformation modes.

Herein we report a simple and reliable strategy to fabricate shape-transforming composite hydrogel sheets that are integrated with light-responsive domains with controlled distributions in

[a] Department of Chemistry and Biochemistry, University of Maryland, College Park, MD, 20742, USA. E-mail: znie@umd.edu
[b] Laboratory of Molecular Imaging and Nanomedicine (LOMIN), National Institute of Biomedical Imaging and Bioengineering (NIBIB), National Institutes of Health, USA
[c] MIIT Key Laboratory of Critical Materials Technology for New Energy Conversion and Storage, State Key Laboratory of Urban Water Resource and Environment, School of Chemistry and Chemical Engineering, Harbin Institute of Technology, Harbin 150001, China
[d] Department of Chemical and Biomolecular Engineering, University of Maryland, College Park, MD, 20742, USA

† Electronic supplementary information (ESI) available. See DOI: 10.1039/c8tb01959b

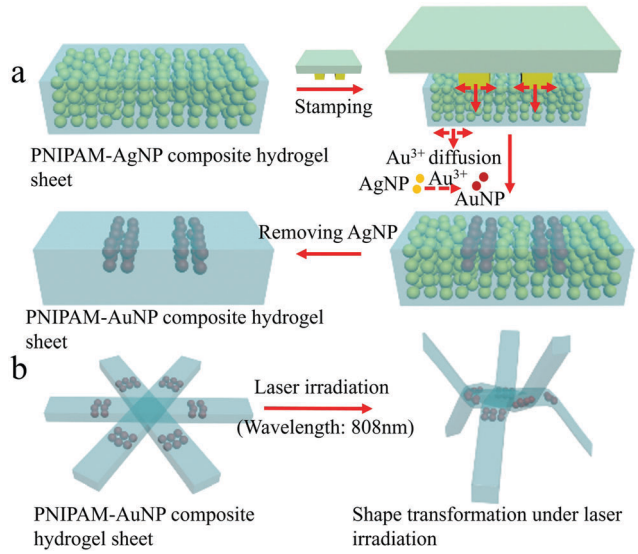

Scheme 1 (a) Schematic illustration of patterning plasmonic AuNPs in both the lateral and *z*-direction of the thermo-responsive hydrogel matrix. (b) NIR light-induced deformation of a 2D composite hydrogel sheet patterned with a photothermal contrast agent (*i.e.*, AuNPs) into a 3D geometry.

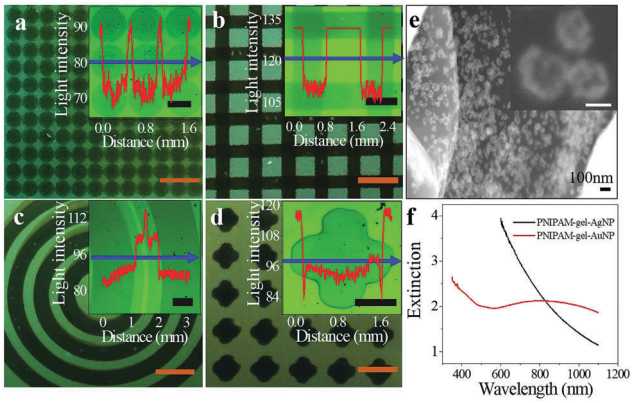

Fig. 1 (a–d) Composite hydrogel sheet patterned with plasmonic AuNP regions of different shapes by a stamping approach. Insets are optical microscopic images of the patterns and light intensity profiles of the patterned domains along the direction indicated by the blue arrow. (e) SEM image of the generated AuNPs with porous hollow features. (f) UV-vis spectra of a hydrogel hybrid before (black curve) and after stamping (red curve). Scale bars are 2 mm in (a–d) and 0.5 mm in the insets of (a–d), and 40 nm in the inset of (e).

both the lateral and *z*-direction of a thermo-responsive hydrogel. The approach was based on contact printing of gold ions into a hydrogel sheet pre-embedded with spherical silver nanoparticles (AgNPs) that have absorption in the visible range and subsequent diffusion-controlled galvanic replacement reaction between gold ions and AgNPs to produce hollow gold nanoparticles (AuNPs) with near-infrared (NIR) absorption (Scheme 1). After removing unreacted AgNPs, the resulting AuNPs were retained in the hydrogel. This approach allows us to control the distribution of light-responsive domains (*i.e.*, photothermal contrast agent of AuNPs) in both the lateral and *z*-direction of the hydrogel matrix by modulating the gold ion diffusion. The composite hydrogel exhibits distinct deformation modes upon NIR light irradiation, depending on irradiation direction and spatial distribution of the AuNP domain. This shape-transforming scenario has rarely been reported previously.

In brief, an agarose hydrogel stamp pre-soaked in a gold ion solution was brought into conformal contact with a AgNP-embedded hydrogel matrix. The AgNP-loaded composite hydrogel matrix was prepared by redox polymerization of an aqueous mixture containing AgNPs, *N*-isopropylacrylamide (NIPAM) monomer, *N*,*N*-methylenebis(acrylamide) cross-linker, ammonium persulfate, and *N*,*N*,*N*′,*N*′-tetramethylethylenediamine (TEMED) catalyst (see the ESI† for details). The number density of AgNPs in the original hydrogel is estimated to be 5.6×10^{11}/mL (see the ESI† for calculations). As the stamp contacted the composite hydrogel, gold ions diffused into the composite hydrogel *via* a concentration-driven diffusion mechanism. During gold ion diffusion, the galvanic replacement reaction between the gold ions and AgNPs regioselectively turned the AgNPs into AuNPs *in situ* within the hydrogel. The unreacted AgNPs were subsequently etched away by using an aqueous solution of $NH_3{\cdot}H_2O$ and H_2O_2 as a wet etchant, leaving AuNPs in the hydrogel. Various patterns with desired feature size (~500 micron) and spacing (~1 mm) were generated by using this approach with the potential of further increasing its resolution (see Fig. 1a–d). The high edge resolution in the AuNP patterns is evidenced by the sharp light intensity transitions between AuNP-containing and AuNP-free regions (see inset graphs in Fig. 1a–d). This approach could be readily scaled up. A 2 cm by 2 cm array of AuNP dots was patterned in the hydrogel to demonstrate the scale-up potential of this approach (see Fig. S1, ESI†). The AuNPs generated by the galvanic replacement reaction had hollow porous structures,[49] as evidenced by SEM characterization (Fig. 1e). After reaction, the AuNP-containing composite hydrogel showed broad light absorption in the NIR range (Fig. 1f), presumably due to the varied morphologies of the resulting porous hollow AuNPs in the gel (Fig. 1e). In contrast, the original AgNP-loaded gel exhibited a lower absorption in the NIR range due to the solid spherical morphology of the AgNPs (Fig. 1f and Fig. S2, ESI†).

The unique feature of our approach to pattern AuNPs in hydrogels is that the AuNP domain size in both the lateral and *z*-direction of the hydrogel can be controlled by varying the stamping time and $HAuCl_4$ precursor concentration (Fig. 2). Fig. 2a–c clearly indicated the variation of AuNP domain size with respect to $HAuCl_4$ concentration in both the lateral and *z*-direction of the hydrogel, demonstrating the excellent control over the spatial distribution of AuNP domains in the hydrogel. The pattern depth and width of AuNPs can be controlled by varying the $HAuCl_4$ precursor and stamping time (Fig. 2d and e). For instance, the depth and width of the AuNP domains increased from 660 μm to 880 μm (Fig. 2d) and increased from 260 μm to 360 μm (Fig. 2e), respectively, with increase of stamping time from 1 minute to 2 minutes at a $HAuCl_4$ concentration of 10 mM. Such fine control over AuNP domain size in the *z*-direction of

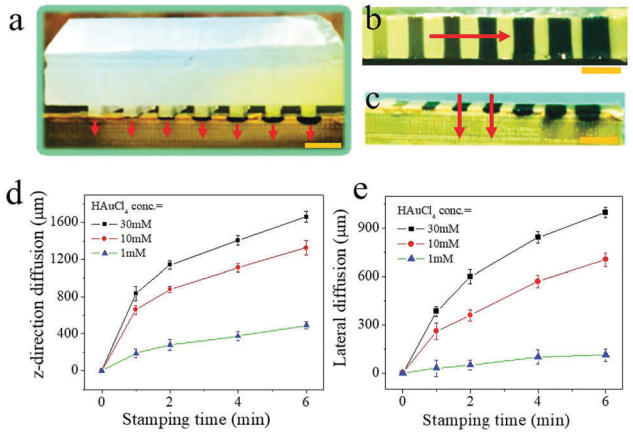

Fig. 2 Analysis of the diffusion-reaction process during stamping. (a) The contact printing of a stamp soaked with gold ion solutions of different concentrations (increasing from left to right) on a hydrogel sheet. The red arrows indicate the propagation direction of the AuNP domain along the thickness direction of the sheet. (b and c) Top view (b) and side view (c) of the hydrogel after stamping. Arrows indicate the direction of increasing density or size of the AuNP domains generated in the hydrogel; (d and e) time-dependent variation of AuNP domain size in the z-direction and lateral direction of the hydrogel. Scale bars are 2 mm in (a–c).

the material by using the diffusion-controlled method cannot be readily achieved by other approaches such as microcontact printing[50] and photon lithography.[51]

The AuNP-patterned hybrid hydrogel sheet transformed to 3-D geometries under 808 nm laser irradiation, due to localized shrinkage of the thermo-sensitive composite hydrogel arising from the photothermal heating of AuNPs.[42,52–54] The deformed hydrogel returned to its original state in 2 minutes after removing the laser (see Fig. S3b, ESI†). The bending/recovering could be repeated many times without appreciable change in bending angle, demonstrating high reversibility of the deformation (see Fig. S4, ESI†).

To study its bending behaviour as a function of laser power density (PD), the composite hydrogel sheet was patterned to have a bilayer-type structure as illustrated in Fig. 3a. Here the bilayer sheet consists of a hybrid gel layer (containing AuNP domain) with a thickness of h_{hybrid} and a pure gel layer (without AuNPs) with a thickness of h_{pure} (Fig. 3a). As shown in Fig. 3b, when h_{hybrid}/h_{pure} = 0.3, the bending curvature of the composite hydrogel sheet increased with increase of PD. When $h_{hybrid}/h_{pure} \geq 0.6$, the bending curvature exhibited a peak as a

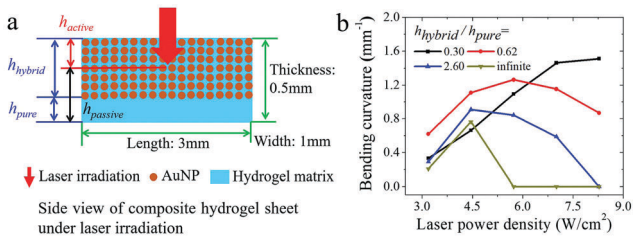

Fig. 3 (a) Schematic illustration of the cross-section of the composite hydrogel sheet under laser irradiation. (b) Bending analysis of the composite hydrogel sheet as a function of laser power density.

function of laser PD. These bending behaviours can be explained by using the classical model developed for bending deformation of bi-metal thermostats. The bending curvature of the hydrogel sheet (κ) is described as,[55,56]

$$\kappa = 6\frac{eh(1+h)\Delta\xi}{h_{total}(1+4eh+6eh^2+4eh^3+e^2h^4)}$$

where h_{total}, e, h and $\Delta\xi$ are the thickness of the composite hydrogel sheet, the ratio between the Young's modulus of the active and passive gel layer, the ratio between the thickness of the active and passive gel layer and the actuation force, respectively. Here the actuation force is the volumetric swelling ratio difference between the active and passive gel layer. This model has been used previously to interpret bending of shape-changing hydrogel materials.[16,57] We note that the magnitude change in e during laser irradiation does not produce a substantial effect on the bending curvature of the composite hydrogel sheet (see the ESI† for calculation details). This observation is in good agreement with our prediction by the model and conclusion drawn in a previous report[56] (see more detailed discussion in the ESI†). Therefore, we consider e as a constant and study the effects of h and $\Delta\xi$ on the bending curvature of the composite hydrogel sheet in the following discussion.

In the bending deformation of our composite sheet, the active gel layer is the layer that absorbs light and generates heat, while the passive gel layer is the layer that does not absorb laser energy (Fig. 3a). Due to laser intensity decay (caused by strong absorption of AuNPs in the hydrogel sheet) along the irradiation direction, the thickness of the active and passive gel layer (h_{active}, $h_{passive}$, Fig. 3a) varied depending on the thickness of the hybrid gel layer and laser PD. When h_{hybrid}/h_{pure} = 0.3, light can access all the hybrid gel layer. In this case, since $h = h_{active}/h_{passive}$ = 0.3 ($h_{active} = h_{hybrid}$, $h_{passive} = h_{pure}$) is a constant, the increase in laser PD led to an increase in $\Delta\xi$ (see Fig. S5b, ESI†) and hence increase in bending curvature. In contrast, at high h_{hybrid}/h_{pure}, light can only penetrate part of the hybrid layer due to strong light absorption by AuNPs and intensity decay along the hydrogel's thickness direction. The light penetration depth increased with increase of laser PD, leading to an increase of $h = h_{active}/h_{passive}$. As a result, the dependency curve of bending curvature on laser PD exhibited a parabolic form.[57] The bending curvature was found to increase with decreasing gel thickness (see Fig. S6 and S7, ESI†). This result is in good agreement with the model, since a smaller h_{total} of a thinner gel gives rise to a larger κ when other parameters (h, e and $\Delta\xi$) are the same.

We note that the surface temperature of a pure PNIPAM hydrogel only slightly increased upon laser irradiation, thus leading to negligible deformation of the hydrogel (Fig. S8 and S9a, ESI†). In contrast, a hybrid PNIPAM hydrogel heated up substantially and bent appreciably under the same conditions of laser irradiation (Fig. S8 and S9b, ESI†). These results suggest that the presence of a hybrid layer in the composite hydrogel plays a central role in its shape transformations.

Finally, we fabricated composite hydrogel sheets with varied AuNP patterns (Fig. 4). In these composite sheets, AuNPs were

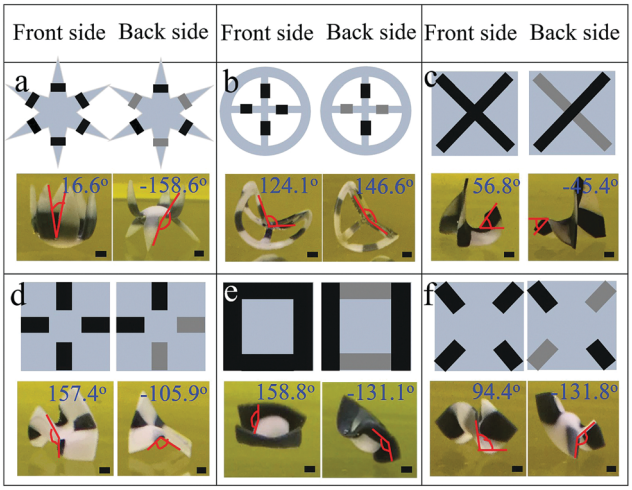

Fig. 4 Shape deformation of a patterned composite hydrogel sheet under continuous laser irradiation (wavelength: 808 nm). The black and grey regions represent areas with AuNPs patterned throughout the hydrogel and partially into the hydrogel along the thickness direction, respectively. The negative bending angle indicates that the bending direction was opposite when the laser was irradiated onto the hybrid hydrogel from different sides (front side *vs.* back side). The total thickness (h_{total}) of the composite hydrogel sheet and thickness of the hybrid gel layer (h_{hybrid}) are: (a) h_{total} = 0.25 mm, h_{hybrid} = 0.18 mm; (b) h_{total} = 0.50 mm, h_{hybrid} = 0.46 mm; (c) h_{total} = 0.25 mm, h_{hybrid} = 0.23 mm; (d) h_{total} = 0.25 mm, h_{hybrid} = 0.08 mm; (e) h_{total} = 0.25 mm, h_{hybrid} = 0.22 mm; and (f) h_{total} = 0.25 mm, h_{hybrid} = 0.18 mm, respectively. A laser power density of 6.38 W cm^{-2} was used in all cases. Scale bars: 1 mm.

patterned throughout the hydrogel in a certain region (colored black in illustrations in Fig. 4) and partially into the hydrogel in other region (colored grey in illustrations in Fig. 4) along the hydrogel's thickness direction. For simplicity in discussion, we defined the "front side" of the hydrogel as the side that has more AuNP domains and the "back side" as the side that has a smaller number of AuNP domains. As an example, the "front side" of the star-like composite sheet has six AuNP domains while its "back side" has three AuNP domains (Fig. 4a).

We found that the patterned composite hydrogel sheet had distinct deformation behaviours, depending on which hydrogel side was irradiated (Fig. 4). As an example, when the "front side" of the patterned star-like hydrogel sheet was irradiated, all six petals bent in the same direction; while they bent in opposite directions when its back side was irradiated (see Fig. 4a and Videos 1, 2, ESI†). This is because when irradiated from the "back side" of the star-like hydrogel sheet, the three petals with AuNP domains on this side bent towards the laser while the other three petals bent away from the laser since the AuNP domains were located on their "front side". The deformations of composite sheets with other AuNP patterns are affected by light exposure direction as well (Fig. 4b–f). For example, when the "front side" was irradiated, the square-shaped composite hydrogel sheet with AuNPs patterned on its corner transformed to a saddle geometry; while it deformed to an incomplete tube-like structure when its "back side" was irradiated (Fig. 4f). As far as we know, this deformation scenario has not been reported previously.

Conclusions

We report a simple and reliable approach to pattern photo-thermal contrast agents (*i.e.*, AuNPs) spatially in a thermo-responsive hydrogel matrix by using contact printing of metal precursors and galvanic replacement of AgNPs pre-embedded in the hydrogel matrix. The distribution of AuNPs in both the lateral and *z*-direction of the hydrogel can be controlled by varying the diffusion and reaction of stamped chemicals. The composite hydrogel sheet transformed to 3-D geometries under continuous NIR laser irradiation by the combination of the photo-thermal effect of the AuNPs and the thermo-responsive property of the hydrogel matrix. This approach allowed us to design composite hydrogels that exhibited distinct transformation modes, depending on the laser irradiation direction, which has rarely been reported previously. We foresee that the patterning technique reported here is general and can be applied to other thermo-responsive hydrogel systems, while the patterned composite hydrogels may find applications in biomedicine[10,58] and soft robotics.[17,21,22]

Conflicts of interest

There are no conflicts to declare.

Acknowledgements

Z. N. gratefully acknowledges the financial support of the National Science Foundation (grants: DMR-1255377, CHE-1505839). We also acknowledge the support of the Maryland NanoCenter and its NispLab. The NispLab is supported in part by the NSF as an MRSEC Shared Experimental Facility. (Supporting Information is available online from Royal Society of Chemistry or from the author).

References

1 R. Kempaiah and Z. H. Nie, *J. Mater. Chem. B*, 2014, **2**, 2357–2368.
2 L. Ionov, *Mater. Today*, 2014, **17**, 494–503.
3 Y. Liu, J. Genzer and M. D. Dickey, *Prog. Polym. Sci.*, 2016, **52**, 79–106.
4 J. Zhou and S. S. Sheiko, *J. Polym. Sci., Polym. Phys.*, 2016, **54**, 1365–1380.
5 S.-J. Jeon, A. W. Hauser and R. C. Hayward, *Acc. Chem. Res.*, 2017, **50**, 161–169.
6 C. Lowenberg, M. Balk, C. Wischke, M. Behl and A. Lendlein, *Acc. Chem. Res.*, 2017, **50**, 723–732.
7 L. Ionov, *Adv. Funct. Mater.*, 2013, **23**, 4555–4570.
8 T. van Manen, S. Janbaz and A. A. Zadpoor, *Mater. Today*, 2018, **21**, 144–163.
9 Q. Zhao, H. J. Qi and T. Xie, *Prog. Polym. Sci.*, 2015, **49-50**, 79–120.
10 K. Malachowski, J. Breger, H. R. Kwag, M. O. Wang, J. P. Fisher, F. M. Selaru and D. H. Gracias, *Angew. Chem., Int. Ed.*, 2014, **53**, 8045–8049.

11 Z. J. Wei, Z. Jia, J. M. Athas, C. Y. Wang, S. R. Raghavan, T. Li and Z. H. Nie, *Soft Matter*, 2014, **10**, 8157–8162.
12 S. H. Jiang, F. Y. Liu, A. Lerch, L. Ionov and S. Agarwal, *Adv. Mater.*, 2015, **27**, 4865–4870.
13 C. Ma, T. Li, Q. Zhao, X. Yang, J. Wu, Y. Luo and T. Xie, *Adv. Mater.*, 2014, **26**, 5665–5669.
14 Z. L. Wu, M. Moshe, J. Greener, H. Therien-Aubin, Z. H. Nie, E. Sharon and E. Kumacheva, *Nat. Commun.*, 2013, **4**, 1586.
15 J. C. Athas, C. P. Nguyen, B. C. Zarkett, A. Gargava, Z. H. Nie and S. R. Raghavan, *ACS Appl. Mater. Interfaces*, 2016, **8**, 19066–19074.
16 A. Cangialosi, C. Yoon, J. Liu, Q. Huang, J. K. Guo, T. D. Nguyen, D. H. Gracias and R. Schulman, *Science*, 2017, **357**, 1126–1129.
17 E. Palleau, D. Morales, M. D. Dickey and O. D. Velev, *Nat. Commun.*, 2013, **4**, 2257.
18 H. Arazoe, D. Miyajima, K. Akaike, F. Araoka, E. Sato, T. Hikima, M. Kawamoto and T. Aida, *Nat. Mater.*, 2016, **15**, 1084–1089.
19 M. M. Ma, L. Guo, D. G. Anderson and R. Langer, *Science*, 2013, **339**, 186–189.
20 R. Luo, J. Wu, N.-D. Dinh and C.-H. Chen, *Adv. Funct. Mater.*, 2015, **25**, 7272–7279.
21 E. Wang, M. S. Desai and S. W. Lee, *Nano Lett.*, 2013, **13**, 2826–2830.
22 J. K. Mu, C. Y. Hou, H. Z. Wang, Y. G. Li, Q. H. Zhang and M. F. Zhu, *Sci. Adv.*, 2015, **1**, e1500533.
23 D. Han, C. Farino, C. Yang, T. Scott, D. Browe, W. Choi, J. W. Freeman and H. Lee, *ACS Appl. Mater. Interfaces*, 2018, **10**, 17512–17518.
24 D. Morales, E. Palleau, M. D. Dickey and O. D. Velev, *Soft Matter*, 2014, **10**, 1337–1348.
25 J. A. Lv, Y. Y. Liu, J. Wei, E. Q. Chen, L. Qin and Y. L. Yu, *Nature*, 2016, **537**, 179–184.
26 S. Palagi, A. G. Mark, S. Y. Reigh, K. Melde, T. Qiu, H. Zeng, C. Parmeggiani, D. Martella, A. Sanchez-Castillo, N. Kapernaum, F. Giesselmann, D. S. Wiersma, E. Lauga and P. Fischer, *Nat. Mater.*, 2016, **15**, 647–653.
27 A. H. Gelebart, D. Jan Mulder, M. Varga, A. Konya, G. Vantomme, E. W. Meijer, R. L. B. Selinger and D. J. Broer, *Nature*, 2017, **546**, 632–636.
28 X. L. Lu, S. W. Guo, X. Tong, H. S. Xia and Y. Zhao, *Adv. Mater.*, 2017, **29**, 1606467.
29 O. M. Wani, H. Zeng and A. Priimagi, *Nat. Commun.*, 2017, **8**, 15546.
30 Y. Yang, Z. Q. Pei, Z. Li, Y. Wei and Y. Ji, *J. Am. Chem. Soc.*, 2016, **138**, 2118–2121.
31 S. Iamsaard, S. J. Asshoff, B. Matt, T. Kudernac, J. Cornelissen, S. P. Fletcher and N. Katsonis, *Nat. Chem.*, 2014, **6**, 229–235.
32 S. J. Asshoff, F. Lancia, S. Iamsaard, B. Matt, T. Kudernac, S. P. Fletcher and N. Katsonis, *Angew. Chem., Int. Ed.*, 2017, **56**, 3261–3265.
33 A. H. Gelebart, D. J. Mulder, G. Vantomme, A. Schenning and D. J. Broer, *Angew. Chem., Int. Ed.*, 2017, **56**, 13436–13439.
34 T. J. White and D. J. Broer, *Nat. Mater.*, 2015, **14**, 1087–1098.
35 T. T. Chen, H. Li, Z. H. Li, Q. Jin and J. Ji, *Mater. Horiz.*, 2016, **3**, 581–587.
36 F. J. Ge, X. L. Lu, J. Xiang, X. Tong and Y. Zhao, *Angew. Chem., Int. Ed.*, 2017, **56**, 6126–6130.
37 Y. Liu, B. Shaw, M. D. Dickey and J. Genzer, *Sci. Adv.*, 2017, **3**, e1602417.
38 J. W. Chen, F. K. C. Leung, M. C. A. Stuart, T. Kajitani, T. Fukushima, E. van der Giessen and B. Feringa, *Nat. Chem.*, 2018, **10**, 132–138.
39 B. Adhikari, Y. Yamada, M. Yamauchi, K. Wakita, X. Lin, K. Aratsu, T. Ohba, T. Karatsu, M. J. Hollamby, N. Shimizu, H. Takagi, R. Haruki, S. Adachi and S. Yagai, *Nat. Commun.*, 2017, **8**, 15254.
40 H. Y. Guo, J. Cheng, J. Y. Wang, P. Huang, Y. J. Liu, Z. Jia, X. Y. Chen, K. Y. Sui, T. Li and Z. H. Nie, *J. Mater. Chem. B*, 2017, **5**, 2883–2887.
41 A. W. Hauser, A. A. Evans, J. H. Na and R. C. Hayward, *Angew. Chem., Int. Ed.*, 2015, **54**, 5434–5437.
42 Z. C. Zhu, E. Senses, P. Akcora and S. A. Sukhishvili, *ACS Nano*, 2012, **6**, 3152–3162.
43 H. W. Huang, M. S. Sakar, A. J. Petruska, S. Pane and B. J. Nelson, *Nat. Commun.*, 2016, **7**, 12263.
44 L. D. Zhang, H. R. Liang, J. Jacob and P. Naumov, *Nat. Commun.*, 2015, **6**, 7429.
45 Y. Yang, Y. Tan, X. L. Wang, W. L. An, S. M. Xu, W. Liao and Y. Z. Wang, *ACS Appl. Mater. Interfaces*, 2018, **10**, 7688–7692.
46 H. Therien-Aubin, Z. L. Wu, Z. H. Nie and E. Kumacheva, *J. Am. Chem. Soc.*, 2013, **135**, 4834–4839.
47 H. Therien-Aubin, M. Moshe, E. Sharon and E. Kumacheva, *Soft Matter*, 2015, **11**, 4600–4605.
48 A. H. Gelebart, D. J. Mulder, M. Varga, A. Konya, G. Vantomme, E. W. Meijer, R. L. B. Selinger and D. J. Broer, *Nature*, 2017, **546**, 632–636.
49 Y. G. Sun and Y. N. Xia, *J. Am. Chem. Soc.*, 2004, **126**, 3892–3901.
50 V. Santhanam and R. P. Andres, *Nano Lett.*, 2004, **4**, 41–44.
51 S. Shukla, X. Vidal, E. P. Furlani, M. T. Swihart, K. T. Kim, Y. K. Yoon, A. Urbas and P. N. Prasad, *ACS Nano*, 2011, **5**, 1947–1957.
52 Y. Zhou, A. W. Hauser, N. P. Bende, M. G. Kuzyk and R. C. Hayward, *Adv. Funct. Mater.*, 2016, **26**, 5447–5452.
53 B. M. Budhlall, M. Marquez and O. D. Velev, *Langmuir*, 2008, **24**, 11959–11966.
54 M. Das, N. Sanson, D. Fava and E. Kumacheva, *Langmuir*, 2007, **23**, 196–201.
55 L. B. Freund, J. A. Floro and E. Chason, *Appl. Phys. Lett.*, 1999, **74**, 1987–1989.
56 S. Timoshenko, *J. Opt. Soc. Am.*, 1925, **11**, 233–255.
57 R. M. Erb, J. S. Sander, R. Grisch and A. R. Studart, *Nat. Commun.*, 2013, **4**, 1712.
58 G. Stoychev, C. Reuther, S. Diez and L. Ionov, *Angew. Chem., Int. Ed.*, 2016, **55**, 16106–16109.

Supporting information

Shape-shifting composite hydrogel sheet with spatially patterned plasmonic nanoparticles

Hongyu Guo[a], Yijing Liu[b], Yang Yang[a], Guangyu Wu[a,c], Kerry Demella[d], Srinivasa R. Raghavan[d] and Zhihong Nie[a*]

[a]Department of Chemistry and Biochemistry, University of Maryland, College Park, MD 20742, USA

[b]Laboratory of Molecular Imaging and Nanomedicine (LOMIN), National Institute of Biomedical Imaging and Bioengineering (NIBIB), National Institutes of Health, USA

[c]MIIT Key Laboratory of Critical Materials Technology for New Energy Conversion and Storage, State Key Laboratory of Urban Water Resource and Environment, School of Chemistry and Chemical Engineering, Harbin Institute of Technology, Harbin 150001, China

[d]Department of Chemical and Biomolecular Engineering, University of Maryland, College Park, MD 20742, USA

* Corresponding author. E-mail: znie@umd.edu

Experimental section

Materials. All chemicals were purchased from Sigma-Aldrich unless otherwise noted and the chemicals were used without further treatment. Chemicals used were as follows: N-Isopropylacrylamide (NIPAM, monomer), N,N'-Methylenebis(acrylamide) (BIS, cross-linker,), Ammonium persulfate (APS, initiator), N,N,N',N'-Tetramethylethylenediamine (TEMED, catalyst), Silver nitrate ($AgNO_3$), Polyvinylpyrrolidone (PVP, MW 55000), Gold(III) chloride trihydrate ($HAuCl_4$), Ethylene glycol (EG), Ammonium hydroxide (25.0%-28.0%). Hydrogen peroxide (30% solution) was purchased from EMD Millipore Cooperation. Agarose powder was purchased from EZ BioResearch. Polydimethylsiloxane (PDMS) elastomer kit (Sylgard 184) was bought from Dow Corning. Deionized water was used throughout the experiments.

Synthesis of Silver Nanoparticle (AgNP). Silver nanoparticle was synthesized according to ref.1 (Synthesis of Ag Seeds section) in this supporting information.

Synthesis of AgNP-Loaded Hydrogel. The AgNP-loaded hydrogel was fabricated by a redox method. Typically, 0.113g NIPAM monomer and 0.008g BIS cross-linker were dissolved in 500 μL AgNP aqueous solution. After adding 5 μL 10 wt% APS aqueous solution, the hydrogel precursor solution was put on ice bed for 5 minutes. Then 0.1 μL TEMED was added and mixed with the monomer solution. After mixing, the monomer solution was injected into a pre-made mold made of two glass slides and a spacer. The gelation took place at room temperature in a few minutes and the glass mold was then put in 4 ^{o}C refrigerator for the gelation to proceed further for 2 hours. After 2 hours, the glass mold was immersed in water and was open to release the AgNP-loaded hydrogel. The AgNP-loaded hydrogel was kept in a large amount of water for one day to leak out unreacted chemicals.

Fabrication of Agarose Stamp. The agarose stamp was made by gelating agarose aqueous solution on a PDMS mold. In a representative fabrication process, a poly(lactic acid) (PLA) plastic mold with bas-relief features was first printed out by using 3D printer (Original Prusa i3 MK2S).

Then PDMS was cured on this mold at 70 ^{o}C for 1 hour. The cured PDMS with opposite features was peeled off from PLA mold. After that, the PDMS mold surface was made hydrophilic by subjecting it to air plasma for three minutes. Then 4 wt% hot agarose aqueous solution was casted onto PDMS mold and cooled at room temperature to gelate. After gelation, the agarose gel with bas-relief features was peeled off from the PDMS mold. This agarose gel was then used in wet stamping process.

Wet Stamping. The agarose gel with base-relief features was first immersed in gold precursor ($HAuCl_4$) aqueous solution for 30 minutes. Then it was taken out and the $HAuCl_4$ precursor on agarose gel surface was removed by using Kimwipes. The agarose stamp was then brought into contact with the surface of AgNP-loaded hydrogel. Once agarose stamp was in contact with AgNP-loaded hydrogel, galvanic replacement reaction between $HAuCl_4$ and AgNP started and gold nanoparticle (AuNP) was generated *in-situ*. By designing features in agarose stamp, different pattern forms of AuNP domains in the hydrogel could be easily obtained. After wet stamping, the unreacted AgNP in the hydrogel was etched away by using an aqueous mixture of ammonium hydroxide and hydrogen peroxide (6:1 in volume ratio), leaving behind AuNP domains in the hydrogel. Without special notification, we used hybrid hydrogel to represent AuNP-containing hydrogel. For fabricating agarose stamp loaded with gold ion of different concentrations, the PDMS mold used to make agarose stamp was utilized as an ink well. Aqueous gold ion solution with different concentrations were injected to the ink well. Then the agarose stamp was aligned with the ink well and was brought in contact with the gold ion solution to absorb gold ions. Finally the stamp was made in contact with AgNP-loaded hydrogel to generate gold nanoparticle domains of various sizes in both xy- and z-direction of the hydrogel.

Diffusion Study. The agarose stamp was brought in contact with the AgNP-loaded hydrogel for different amount of time. Then the AgNP was etched away. The size of the generated nanoparticle domain in both xy- and z-direction of the hydrogel was then analyzed by using optical microscope. The nanoparticle domain size was plotted with respect to stamping time.

Light-Triggered Shape Transformation. An 808 nm laser (MDL-N-808, Changchun New Industries Optoelectronics Technology Co., Ltd, China) with tunable output power (0-8W) was used as the laser source throughout the experiments. During the experiments, the hybrid hydrogel was immersed in 600 mL water in a glass petri dish.

Hydrogel Swelling. The swelling property of the hydrogel was characterized by using the swelling ratio which was measured gravimetrically after wiping off the excess water on the hydrogel's surface with a piece of Kim wipe in the temperature range from 18 to 36 °C. The hydrogel was incubated in a water bath for at least 24 h at each temperature. The swelling ratio was calculated by using the following formula,

$$\text{Swelling ratio} = W_s/W_d$$

where W_s was the weight of the swollen hydrogel at the particular temperature and W_d was the dry weight of the hydrogel.

Mechanical Property. An AR2000 stress-controlled rheometer (TA Instruments) was used to study the mechanical properties of the hybrid hydrogel sheet. Rheological experiments were performed at 25 °C, 28 ^{o}C and 35 °C, respectively by using cone-and-plate geometry (20 mm diameter and 2^{o} cone angle). A solvent trap was used to minimize drying of the sample during measurements. Dynamic stress-sweep experiments were first performed on the sample to identify

its linear viscoelastic (LVE) region at different temperatures and dynamic frequency sweeps were then performed within the LVE region.

UV-VIS Measurement. The optical property of the hydrogel was characterized by measuring its light extinction using UV-VIS spectroscopy (Lambda 40 UV/VIS Spectrometer, PerkinElmer, USA). In the measurement, air was used as reference and a piece of hydrogel was then put on a glass slide. The UV-VIS spectra were then taken at a slit width of 1 nm, scanning speed of 480 nm/min and data interval of 1 nm.

Scanning Electron Microscopy (SEM). For silver nanoparticle (AgNP) characterization, a drop of AgNP aqueous solution was dried on silicon wafer and the dried sample was imaged by using scanning electron microscopy (XL Series-30, Philips, USA). For hybrid hydrogel characterization, the hybrid hydrogel was first freeze-dried and then coated with carbon (JFC-1200 Fine Coater, Japan). Following that, scanning electron microscopy was used to characterize AuNP in the hydrogel.

Photothermal Imaging of Hybrid Hydrogel. The photothermal property of the hybrid hydrogel was studied by photothermal imaging technique. Briefly, the hybrid hydrogel sheet was immersed in 3 mL water in a plastic petri dish and was irradiated with an 808 nm laser at a power density of 6.37 W/cm^2 for 1 min and then the laser was shut off. The surface temperature of the hybrid hydrogel was monitored by using a FLIR SC300 infrared camera (FLIR, Arlington, VA). Real-time thermal images were captured with frame rate at 60 Hz, and analyzed by FLIR Examiner software. We found that the hybrid hydrogel sheet started to deform while its surface temperature increased from 22 °C to 29 °C (Fig.S5a) during the irradiation process and it went back to its original shape when it cooled down.

Surface temperature of pure and hybrid PNIPAM hydrogel under laser irradiation. In the experiment, a piece of pure PNIPAM hydrogel (length: 25mm, width: 20mm, thickness: 2mm) was put on a plastic petri dish (made of polystyrene) in air at room temperature (18.5^{o}C). The hydrogel was irradiated by laser with different power densities for 1 minute. Then the laser was switched off and the surface temperature of the pure hydrogel was measured by using a digital thermometer (MeasuPro Waterproof Digital Food Thermometer). The correlation between surface temperature and laser power density is then plotted. For control experiment, a piece of hybrid PNIPAM hydrogel (length: 30mm, width: 25mm, thickness: 2mm) was also irradiated in air and its surface temperature was measured in the same way as pure hydrogel.

Jumping and Load-lifting of Composite Hydrogel Sheet. The composite hydrogel sheet (length: 20mm, width: 2mm, thickness: 0.25mm) was patterned with two AuNP strips (width: 2mm, thickness: 0.06mm) and it was irradiated by laser. The patterned hydrogel deformed and jumped by releasing the stored energy during its deformation (SV3). The patterned hydrogel was used to lift up load. A 3mg gelatin bead was raised to 1cm high by 18mg composite hydrogel sheet in 30 seconds under laser irradiation (SV4).

Estimation of Minimum Laser Energy Required for Bending to Occur. The composite hydrogel sheet ((length: 20mm, width: 2.2mm, thickness: 0.25mm)) was patterned with AuNP strip as the "hinge" in bending under irradiation. The width of AuNP was 2.2mm, while its length varied. We found that a larger laser power density was needed to initiate bending of composite sheet with a smaller hinge width in water (Fig. S14). We estimated the minimum laser energy (E) required for bending to occur by using the following equation,

$$E = (I_o - I_o * 10^{-Abs})wlt$$

where I_o, *Abs, t, w, l* are the intensity of incoming laser, absorbance of hydrogel sheet, onset time of bending, hinge width and length, respectively. Using this equation, *E* was calculated to be 0.9 J for this hydrogel (see Table S1).

Estimation of AgNP loading in original hydrogel. Loading of AgNP in the original hydrogel is estimated as follows. 0.1g $AgNO_3$ is assumed to be fully reduced to AgNP which is dispersed in 5mL. The mass of silver atom in the 5mL solution is $\frac{0.1g}{169.87g/mol} \times \frac{107.87g}{mol} = 0.0635g$. The volume (*V*) of a single AgNP with a diameter (*d*) of around 80nm (Fig. S2) is,

$$V = \frac{4}{3}\pi(\frac{d}{2})^3 = 2.1 \times 10^{-17}\ cm^3\ or\ mL$$

and mass (*m*) of a single AgNP is $m = \rho_{density}V = \frac{10.53g}{mL} \times 2.1 \times 10^{-17}mL = 2.3 \times 10^{-14}g$.

Then the number (*N*) of AgNP in 5mL solution is $N = \frac{0.0635g}{2.3 \times 10^{-14}g} = 2.8 \times 10^{12}$

The number density (N_v) of AgNP in solution is $Nv = \frac{N}{5mL} = \frac{2.8 \times 10^{12}}{5mL} = 5.6 \times 10^{11}/mL$.

Since one AgNP leads to one AuNP during galvanic replacement, the number density of AuNP in the composite hydrogel will be equal to $5.6 \times 10^{11}/mL$.

Estimation of magnitude change of modulus ratio (*e*) on bending curvature of composite hydrogel sheet. We examined the effect of modulus ratio, *e*, on bending curvature of the composite hydrogel sheet by using the model presented in the manuscript. We found that the magnitude change of *e* does not produce substantial effect on bending curvature of the composite hydrogel sheet, which agreed with the conclusion drawn in ref. 56 in the revised manuscript. The shear modulus of composite hydrogel sheet (active gel layer) as a function of temperature is shown in Table S2 and Fig. S5d, while the shear modulus of passive gel layer is 838 Pa (Table S2 and Fig. S15) at 25 °C. Shear modulus ratio is used to represent Young's modulus ratio (*e*) used in the model. The calculation result is shown below for the case when h=0.3 (h_{total}=0.25mm).

The model says,

$$\kappa = 6\frac{eh(1+h)\Delta\xi}{h_{total}(1+4eh+6eh^2+4eh^3+e^2h^4)} = A\Delta\xi$$

Here we write $\kappa = A\Delta\xi$ to evaluate the contribution of *e* (related to *A*) and $\Delta\xi$ to bending curvature κ.

Data used in calculation is shown in Table S3. The calculation result is shown in Table S4.

As seen from Table S4, the significant increase of bending curvature κ (from 1.79 to 11.13) when increasing temperature (from 28°C to 35°C) in hybrid gel layer at h=0.3 (corresponding to increasing laser power density) is because of great increase of $\Delta\xi$ (from 0.43 to 2.5), instead of magnitude change of e (from 2.65 to 4.58). This suggested that magnitude change of e during laser irradiation does not produce substantial effect on bending curvature of composite hydrogel sheet.

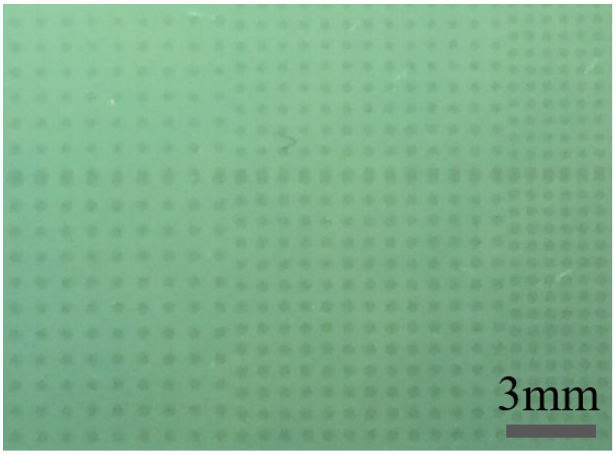

Fig. S1 Large-scale patterning of gold nanoparticles via stamping approach.

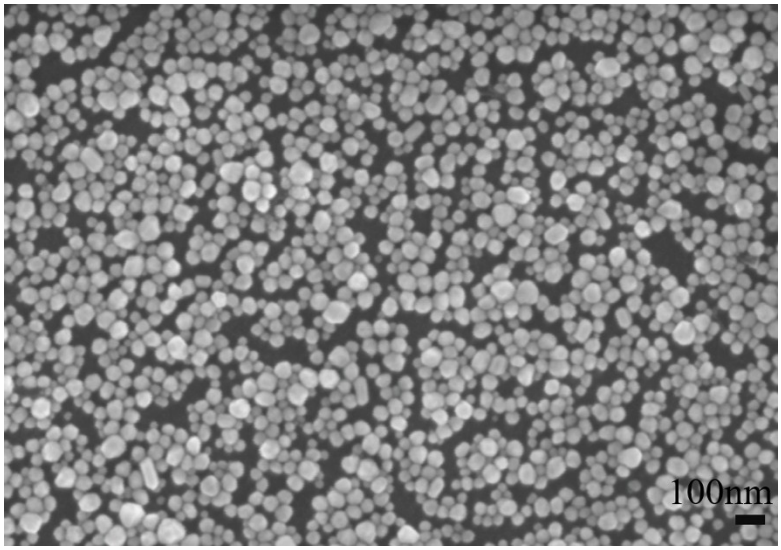

Fig. S2 SEM image of AgNP used to generate AuNP during stamping process.

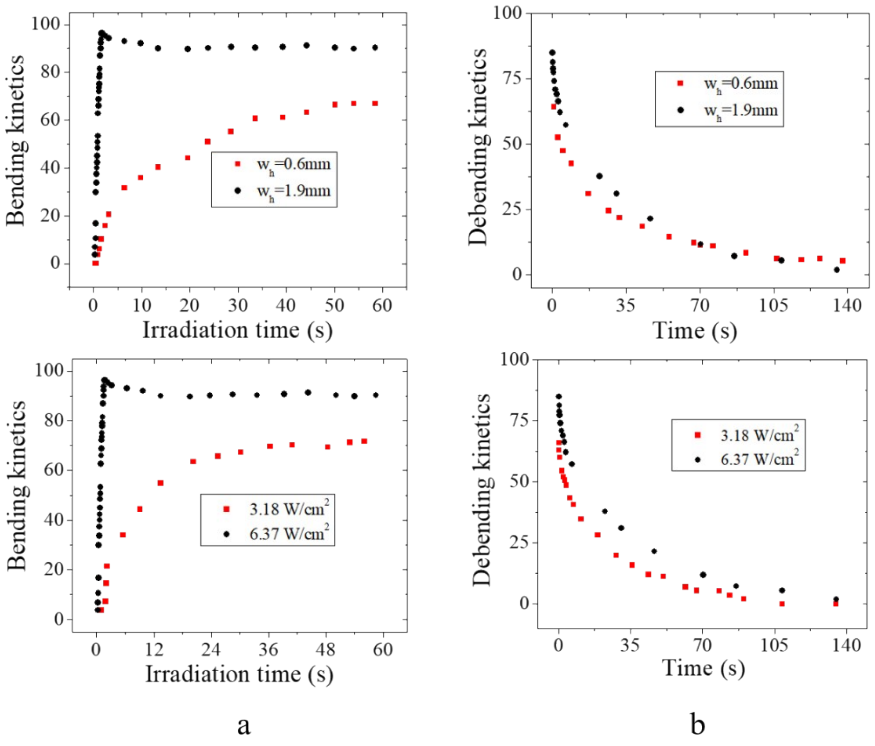

Fig. S3 Bending and recovering kinetics of composite hydrogel with time. w_h was the width of gold nanoparticle domain. The length of gold nanoparticle domain was 2.2mm.

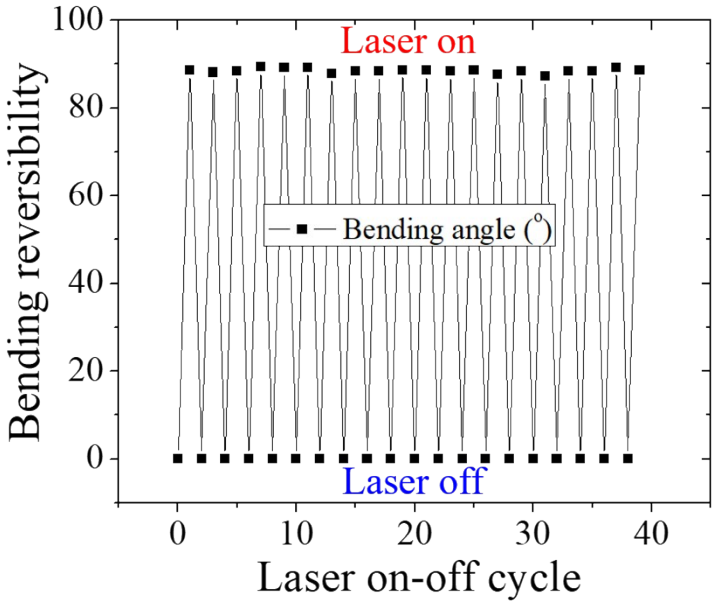

Fig. S4 Bending reversibility of composite hydrogel during laser on-off cycle

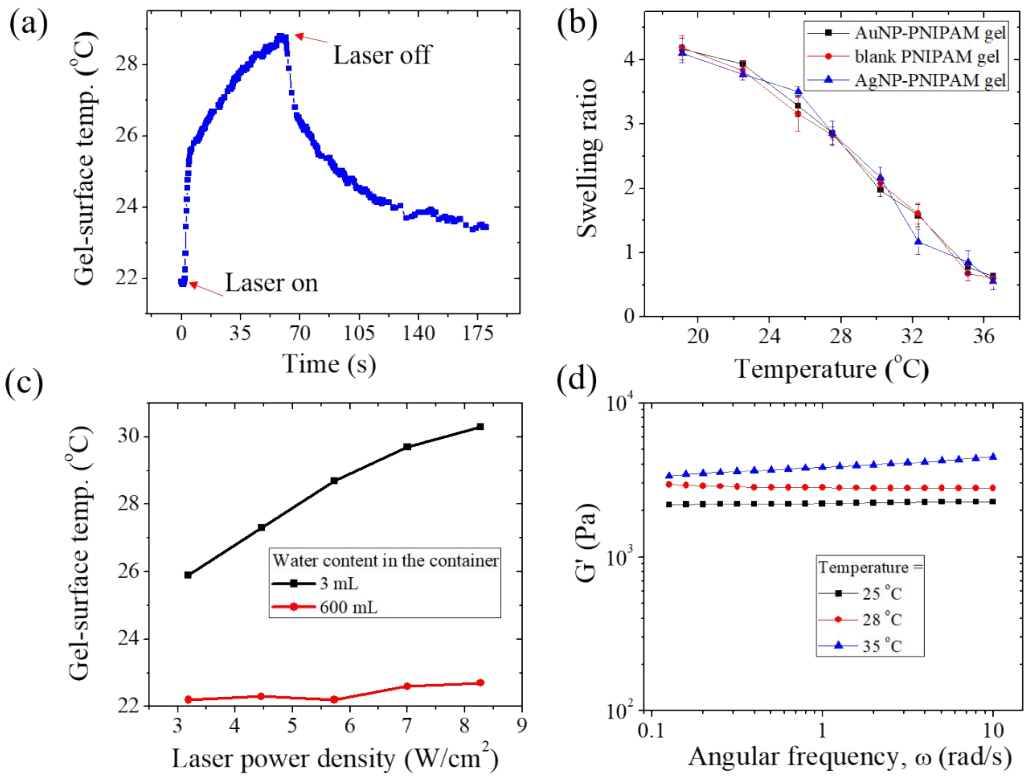

Fig. S5 a) Evolution of surface temperature of composite hydrogel during laser irradiation; b) Swelling of hydrogel as a function of temperature; c) Surface temperature of composite hydrogel as a function of laser power density; d) Shear modulus of composite hydrogel as a function of temperature.

Fig. S6 Bending of composite hydrogel with different thicknesses. The thickness of the composite hydrogel in a) is 0.25mm while it is 0.5mm in b). Thickness of hybrid gel layer is 0.06mm in a) and 0.12mm in b). Scale bar: 2mm.

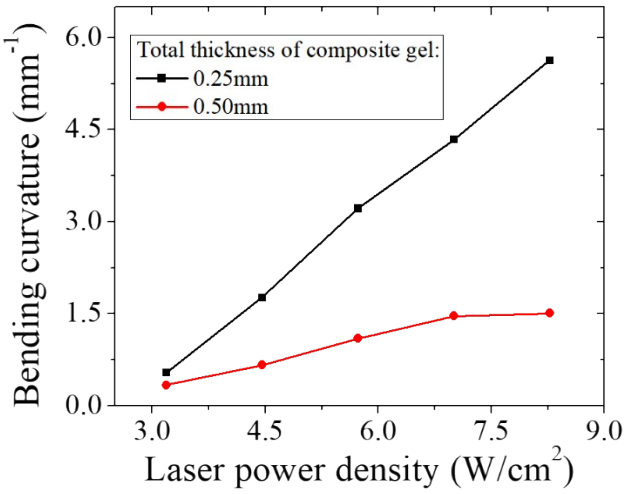

Fig. S7 Quantitative analyses of bending curvature of composite hydrogel with different thicknesses.

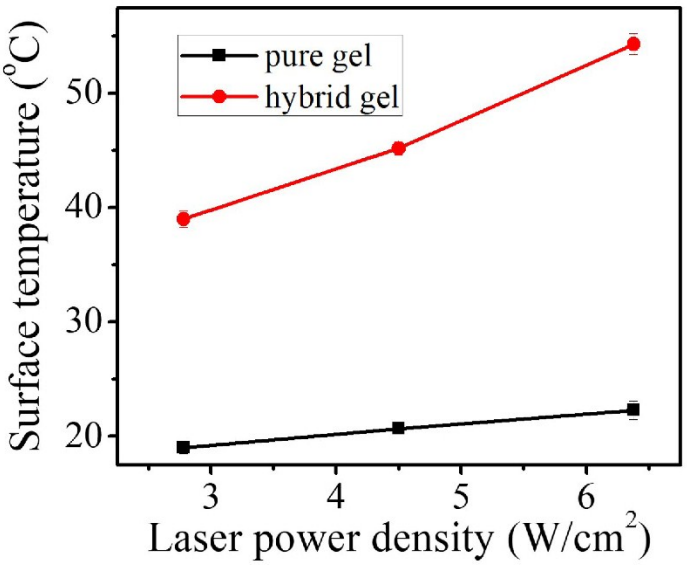

Fig. S8 Surface temperature of pure and hybrid PNIPAM hydrogel as a function of laser power density when irradiated in air. Room temperature is 18.5 °C.

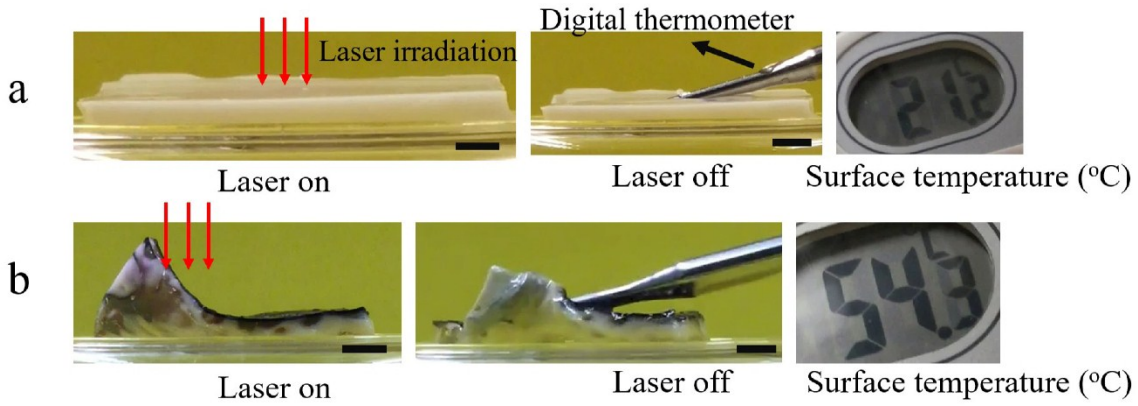

Fig. S9 Shape transformation of pure hydrogel (a) and hybrid hydrogel (b) in air under laser irradiation at 6.38W/cm^2. Thickness of hybrid gel layer in (b) is 200 μm. Scale bar: 4mm.

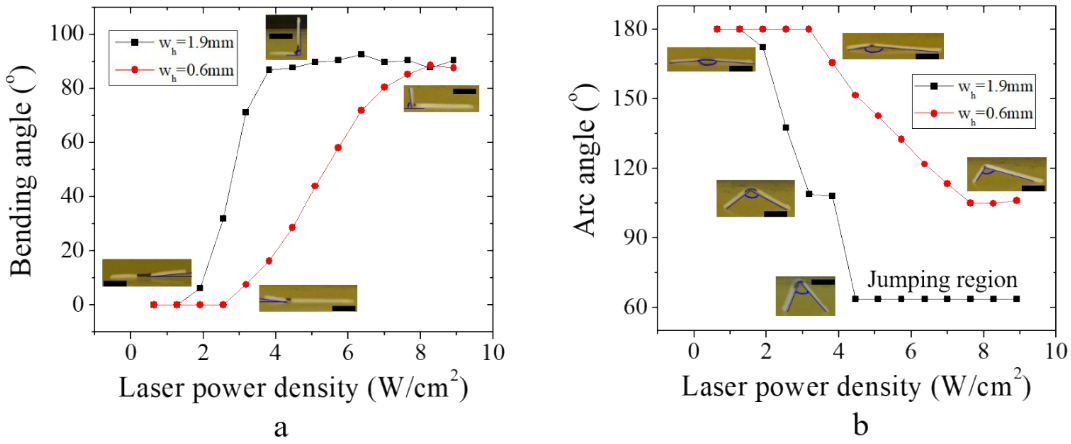

Fig. S10 Bending of composite hydrogel as a function of laser power density. w_h was the width of gold nanoparticle domain. The length of gold nanoparticle domain was 2.2mm. In a) the gold nanoparticle domain faced laser spot while in b) the nanoparticle domain faced away from the laser spot. Scale bar: 5mm.

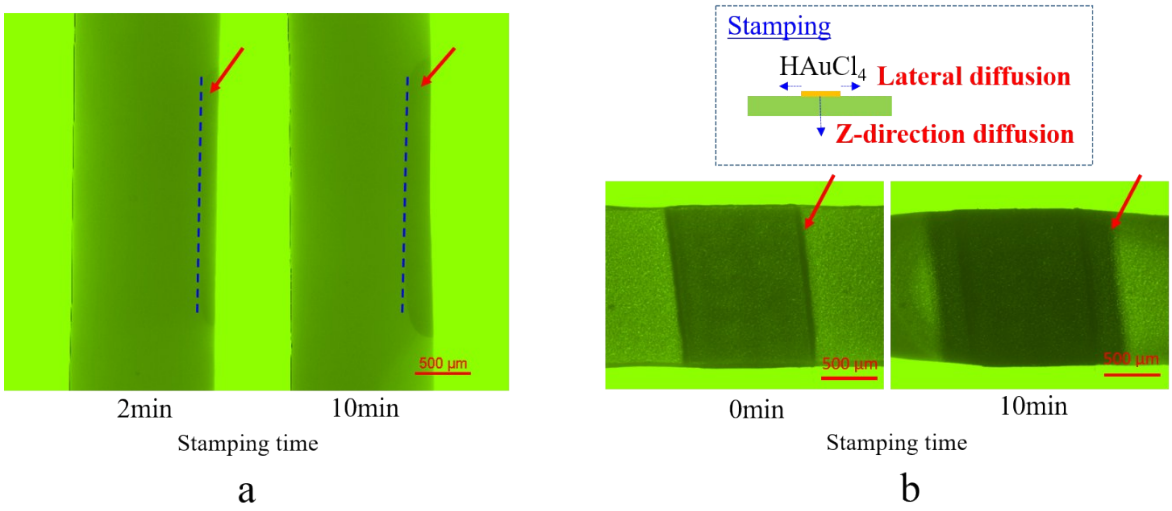

Fig. S11 Optical image showing diffusion-reaction process during stamping. The red arrow indicated the front of the gold nanoparticle domain generated during stamping.

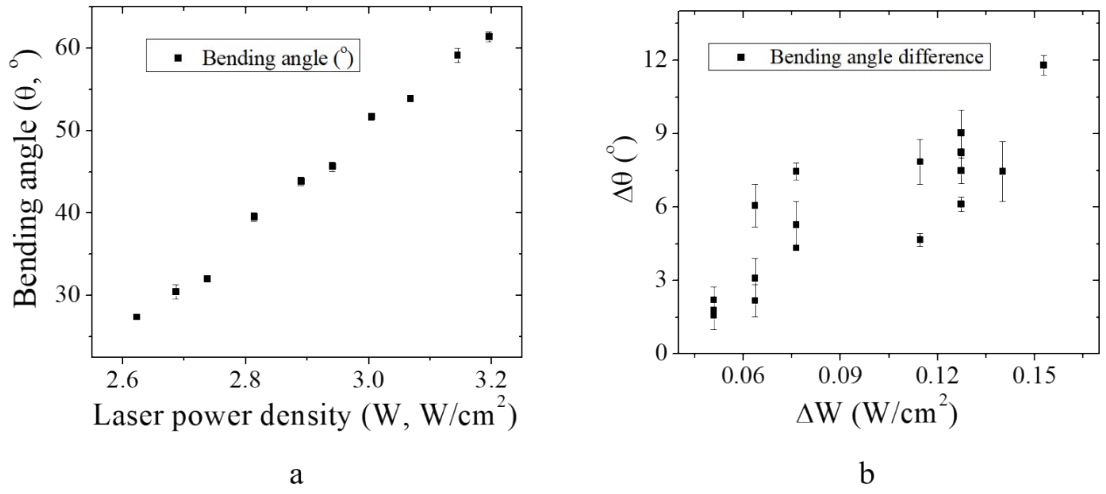

Fig. S12 Bending analysis of composite hydrogel as a function of laser power density. The gold nanoparticle domain had a width of 1.9mm, length of 2.2mm and thickness of 0.06mm. The total thickness of the hybrid hydrogel was 0.25mm.

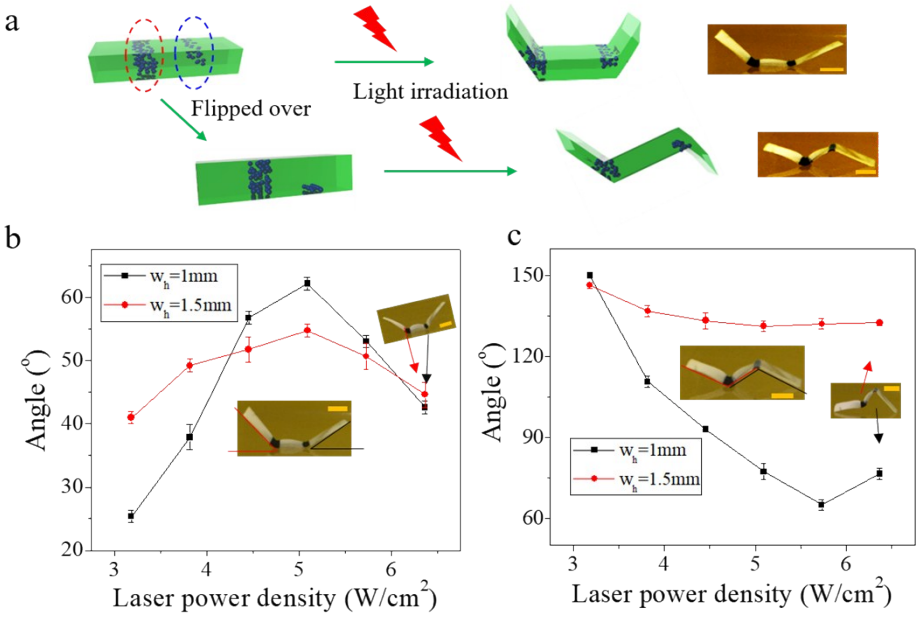

Fig. S13 Bending analysis of composite hydrogel with respect to laser irradiation direction. The composite hydrogel had two rectangular gold nanoparticle (AuNP) strips generated during one-time stamping process. One AuNP strip (w_h=1.5mm) penetrated through gel thickness, while the other one (w_h=1mm) only partially penetrated the gel.

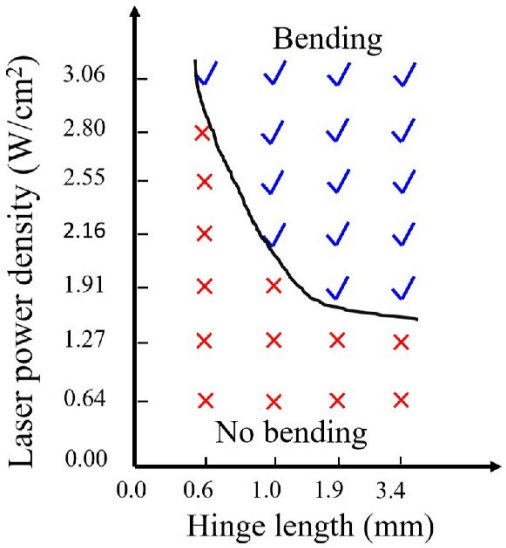

Fig. S14 Bending analysis of composite hydrogel sheet patterned with AuNP strip as hinge in its bending under laser irradiation. Length, width and thickness of composite hydrogel sheet are 20mm, 2.2mm and 0.25mm, respectively. The width of AuNP strip was 2.2mm, while its length varied.

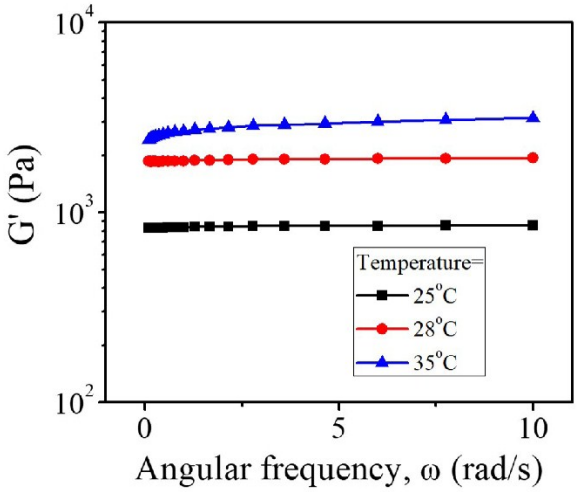

Fig. S15 Shear modulus of pure PNIPAM hydrogel as a function of temperature.

Table S1. Analysis of the minimum energy *E* (J) required for bending to occur.

Hinge length (*l*, mm)	Hinge width (*w*, mm)	Onset time for bending (*t*, s)	Minimum power density (I_o) needed (W/cm^2)	Minimum energy (E) required (J)
0.6	2.3	19	3.06	0.79
1.0	2.1	20	2.16	0.89
1.9	2.2	10	1.91	0.78
3.4	2.2	6	1.91	0.84

Table S2. Shear modulus of pure and hybrid gel layer as a function of temperature.

Temperature (°C)	Shear modulus (G′) of pure gel layer (Pa)	Shear modulus (G′) of hybrid gel layer (Pa)
25	838	2223
28	1879	2842
35	2675	3835

Table S3. Data used in study of effect of e on bending curvature of composite hydrogel sheet; h=0.3, h_{total}=0.25mm.

Temperature (T, °C)	Shear modulus of active gel layer (G, Pa)	Swelling ratio (ξ)
25	2223	3.28
28	2842	2.85
35	3835	0.78

Table S4. Calculation of bending curvature κ based on data in Table S2.

$e = \frac{G_{T,28}}{G_{T,25}}$	$\Delta\xi = \xi_{T,28}$	$A_{(T,28;\ T,25)}$	$\kappa_{(T,28;\ T,25)} = A\Delta\xi$	$e = \frac{G_{T,35}}{G_{T,25}}$	$\Delta\xi = \xi_{T,35} - \xi$	$A_{(T,35;\ T,25)}$	$\kappa_{(T,35;\ T,25)} = A\Delta\xi$
2.65	0.43	4.17	1.79	4.58	2.5	4.45	11.13

References

1. T. S. Rodrigues, A. G. M. da Silva, M. C. Gonçalves, H. V. Fajardo, R. Balzer, L. F. D. Probst, A. H. M. da Silva, J. M. Assaf, P. H. C. Camargo, *Langmuir* **2016,** *32*, 9371.